Article:
Mortimer, A.J., Sander, C.F., Parmar, A.R. et al. (2026) Comparison of AAV9-driven motor neuron transduction following different CNS-directed delivery methods in mice. Scientific Reports. ISSN: 2045-2322

https://doi.org/10.1038/s41598-026-38039-z

Scientific Reports

https://doi.org/10.1038/s41598-026-38039-z

Article in Press

Comparison of AAV9-driven motor neuron transduction following different CNS-directed delivery methods in mice

Received: 14 November 2025

Accepted: 28 January 2026

Published online: 04 March 2026

Cite this article as: Mortimer A.J., Sander C.F., Parmar A.R. *et al.* Comparison of AAV9-driven motor neuron transduction following different CNS-directed delivery methods in mice. *Sci Rep* (2026). https://doi.org/10.1038/s41598-026-38039-z

Alannah J. Mortimer, Chiara F. Sander, Amisha R. Parmar, Ailsa J. Williams, Mimoun Azzouz, Guillaume M. Hautbergue, Pamela J. Shaw, Laura Ferraiuolo & Richard J. Mead

Comparison of AAV9-driven motor neuron transduction following different CNS-directed delivery methods in mice

Alannah J Mole[1]*, Chiara F Sander[1], Amisha R Parmar[1], Ailsa J Williams[1], Mimoun Azzouz[1], Guillaume M Hautbergue[1], Pamela J Shaw[1], Laura Ferraiuolo[1], Richard J Mead[1]*

[1] University of Sheffield, Sheffield Institute for Translational Neuroscience, UK

*Corresponding authors: Richard J Mead, r.j.mead@sheffield.ac.uk, Alannah J Mole: a.j.mole@sheffield.ac.uk

1. Abstract

Gene therapies are promising for diseases previously considered incurable. Adeno-associated virus serotype 9 (AAV9) demonstrates remarkable tropism for motor neurons (MNs) and represents an exciting candidate to target genetic causes of motor neuron diseases like amyotrophic lateral sclerosis (ALS). However, systemic delivery risks immunogenicity and off-target effects, therefore localised delivery to the CNS is advantageous. We assessed MN transduction in wild-type post-natal mice using AAV9-controlled, cytomegalovirus-promoter driven, enhanced GFP expression. Intra-cisterna magna (ICM) and intra-cerebroventricular (ICV) methods were compared. Four weeks post-delivery, GFP positivity in MN and astrocytes were quantified via immunohistochemical approaches and viral genome copy number determined by qPCR. All delivery methods achieved high MN transduction in lumbar spinal cord (>68%). Unilateral ICV delivery provided the highest and most consistent levels (89 ± 3%), and minimal peripheral viral copies. ICV delivery resulted in higher astrocytic transduction, most notably in the cortex. Brainstem MN transduction was high with all methods (>55%). We failed to find evidence of neuronal transduction in motor cortex. Viral genome copies trended higher in spinal cord and brainstem with ICV approaches, however further work is required to understand how bilateral repeated dose delivery leads to more profound increases. Whilst several routes of administration into cerebrospinal fluid exist, direct comparisons for targeting MNs *in vivo* remain limited. Overall, all methods of CNS-directed delivery result in high levels of motor neuron transduction in the lumbar spinal cord and brainstem, but not in motor cortex. Unilateral ICV appears to provide the best balance between consistent, high levels of transduction and low off-target effects. However, ICM might be the better option if seeking to avoid astrocytic transduction.

Keywords: Gene therapy, motor neuron, AAV9, ICM, ICV

2. Highlights

- **CSF delivery of AAV9 targets >68% of lumbar spinal cord (SC) motor neurons**
- **Unilateral ICV yields high and consistent lumbar SC motor neuron transduction (>88%)**
- **Unilateral ICV results in the lowest number of peripheral viral copies**
- **ICV targets significantly more astrocytes, particularly in cortex**
- **Bilateral repeat dose ICV leads to significantly higher viral copies in the liver**

3. List of Abbreviations

Abbreviation	Expansion
AAV	Adeno-associated virus
ALS	Amyotrophic lateral sclerosis
BBB	Blood brain barrier
ChAT	Choline acetyltransferase
CMV	Cytomegalovirus
CSF	Cerebrospinal fluid
GFAP	Glial fibrillary acidic protein
GFP	Green fluorescent protein
IBA1	Ionised calcium binding adaptor molecule 1
ICM	Intra-cisterna magna
ICV	Intra-cerebroventricular
IHC	Immunohistochemistry
IT	Intrathecal
IV	Intravenous
MN	Motor neuron
SMA	Spinal muscular atrophy
vg	Viral genome

4. Introduction

Motor neuron diseases, such as amyotrophic lateral sclerosis (ALS) are devastating neurodegenerative conditions that are characterised by progressive degeneration of motor neurons, leading to debilitating muscle weakness, paralysis, and ultimately death. The unmet need to identify effective therapeutic strategies to target the underlying genetic and molecular abnormalities in ALS has driven the exploration of innovative approaches. The manipulation of genetic material, or gene therapy, to treat or prevent disease, has been transformative in the field of medicine.

Among various gene delivery vectors, adeno-associated virus serotype 9 (AAV9) has gained prominence as an ideal candidate for delivering therapeutic genes to the central nervous system (CNS) [1]. AAV9 has a high affinity for motor neurons, a versatile and safe profile, and has the capacity to cross the blood-brain barrier (BBB) in both rodents and non-human primates, although penetration level varies depending on delivery method [2-7]. AAV9's unique tropism towards the central nervous system has driven extensive work into its application for targeted gene delivery for neurodegenerative conditions, such as the monogenic, childhood motor neuron disease, spinal muscular atrophy (SMA), for which gene therapies are now commercially available [8].

The choice of delivery method of AAV9 plays a crucial role in determining the efficiency and specificity of vector transduction within the CNS. Several strategies have been developed for AAV9 delivery targeted to the CNS including: intravenous (IV) injection; intra-cerebroventricular (ICV) injection; intrathecal (IT) injection either by lumbar puncture or intra-cisterna magna (ICM), sub-pial and intra-parenchymal injection. Each method offers unique advantages and challenges in terms of target cell specificity, transduction efficiency and off-target effects and have been reviewed recently [9]. In brief, intravenous injection can provide systemic distribution of AAV9 vectors, however there are numerous challenges. Firstly, vectors are diluted in the circulation, leading to higher dosing requirements which may have toxicity and cost implications. There is also limited BBB penetration when delivering AAV9 systemically and it may lead to heightened immune response or result in non-specific transduction in peripheral organs [10, 11]. There have also been concerns raised regarding AAV-mediated genotoxicity in the liver, which remains debated in the field, and continues to be monitored in clinical trials [12].

In contrast, direct injection into cerebrospinal fluid (CSF) allows for precise targeting of specific CNS regions or cell populations but may require more invasive procedures that pose risk of tissue damage or immune responses. ICV and ICM methods offer an alternative route for delivery of AAV9 vectors directly into CSF, enabling widespread distribution within the CNS, whilst minimising invasiveness and allowing for lower dosing than systemic delivery. In this study, we chose to deliver vectors early in postnatal development as this is a useful time point for therapeutic proof of concept,

particularly where neurodegenerative phenotypes develop rapidly such as in models of SMA. In addition, at this age, delivery is less invasive, since injections can be delivered without surgery due to skull structure. Despite extensive research on AAV9 vector delivery methods, direct comparative studies evaluating motor neuron and spinal cord transduction after different administration routes in mice after early administration remain limited.

Here, we therefore aimed to compare ICV and ICM methods of AAV9 delivery to mice *in vivo* and compare motor neuron transduction levels to determine the most effective approach for specific motor neuron targeting in pre-clinical studies. We utilised AAV9 controlled cytomegalovirus (CMV)-promoter driven expression of enhanced green fluorescent protein (eGFP) to compare levels of motor neuron transduction in the spinal cord after delivery either ICM, or ICV of neonatal wild-type mice. At around 4 weeks post-infusion, a timepoint at which transgene expression should be high [13, 14], the animal was humanely sacrificed and we used quantitative PCR and immunohistochemical approaches to assess viral distribution. We chose to administer at neonatal stages as this is the major timepoint used in studies for therapeutic proof of concept and particularly where neurodegenerative phenotypes develop rapidly [15]. Whilst this is relevant for paediatric diseases, it could be argued that this might limit translation to adult-onset diseases such as ALS. However, it is worth nothing that there is a growing appreciation for the complexity and functionality of the BBB at early stages in development [16, 17]; recent studies using ICM delivery in cats suggest that motor neuron transduction is not affected by age at CSF delivery [18]. Here, we found that all CNS-directed delivery methods yielded high levels of lumbar spinal cord motor neuron transduction (>68%), however noted that upper motor neurons did not appear transduced in any case. ICM delivery was more variable and technically challenging than ICV but lead to minimal astrocytic transduction. Unilateral ICV delivery targeted lumbar motor neurons at high and consistent levels, along with astrocytes in the cortex. Bilateral ICV delivered over two days (repeat dosing regimen) resulted in significantly higher astrocytic transduction in spinal cord, brainstem and cortex, and resulted in higher peripheral viral genome copies. Overall, we provide direct comparison of methods of motor neuron and spinal cord targeting using AAV9 in neonatal mice.

5. Methods

5.1. Animals and Ethics Statement

All animal procedures and methods were performed in accordance with the UK Animals (Scientific Procedures) Act 1986 under a UK Home Office project license and in line with institutional guidelines and regulations. This license was ethically reviewed and approved by the local ethics committee (University of Sheffield Animal Welfare and Ethical Review Body). Mouse maintenance and day to day care was in line with the Home Office Code of Practice for Housing and Care of Animals Used in Scientific Procedures. The ARRIVE guidelines were followed in the preparation of this paper [19]. Pregnant, wild-type C57BL/6J (JAX®) mice (Charles River,

UK) were housed in open cages in pathogen-free conditions with *ad libitum* access to food and water, on a 12:12 light/dark cycle within animal facilities at the University of Sheffield. Pregnant dams were acclimated to the smell of tattoo ink and isoflurane around one week prior to birthing to familiarise them with these scents and reduce risk of pup rejection. At birth, pups were identified by tattoos that were applied to the footpad under local anaesthetic (EMLA cream) until ear notching was possible. Injections were undertaken before postnatal day (P) 3. Both sexes were used. Runts, which were identified easily on visual inspection, were excluded from the study. At weaning, pups were group housed.

5.2. Injections of viral vector

Self-complimentary (sc) AAV9-CMV-eGFP vector (4815 bp, packaged size 2.2 kb) at titre 9.45E+10 viral genomes (vg)/mouse in 0.001% pluronic carrier, or vehicle only (pluronic) were delivered before postnatal day 3 under general anaesthesia (isoflurane) in the following groups, as summarised in Table 1: 5 µL ICM; 5 µL unilateral (right only) ICV; or 5 µL unilateral (right) ICV on day 1 **and** 5 µL unilateral (left) ICV on day 2 (referred to as ICV bilateral repeat dose). Controls received an equivalent injection of carrier only. Injection material was loaded into a 25 µL Hamilton syringe with 33G, small hub RN needle (PST 4).

Table 1: Summary of treatment groups and titres

Group	Injection site	Injection material	Volume/ injection	Number of injections	Total injection titre
Control	Cisterna magna or lateral ventricle	Pluronic carrier	5 µL	1	0 vg/mouse
ICM	Cisterna magna	scAAV9-CMV-eGFP vector	5 µL	1	9.45E+10 vg/mouse
ICV Unilateral	Lateral ventricle	scAAV9-CMV-eGFP vector	5 µL	1	9.45E+10 vg/mouse
ICV Bilateral Repeat Dose	Lateral ventricle	scAAV9-CMV-eGFP vector	5 µL	2	1.89E+11 vg/mouse

Anaesthesia was induced at 5% isoflurane, and 3 L O^2/min. Pups were transferred onto a Model 940 Small Animal Stereotaxic Instrument (Bilaney) and placed over a WeeSight™ transilluminator to visualise the injection site. Pups were maintained under anaesthesia on a modified nosecone at 2% isoflurane, 0.5 L O^2/min throughout, with alterations based on individual monitoring. For ICM, the injection site was visible through the skin as a small dark triangle and was most easily accessed when the pups head was tilted slightly forward over the transilluminator. Infusions were initiated immediately after the needle punctures through the skin. For ICV, the site was located approximately 0.25 mm lateral to the sagittal suture and 0.50 - 0.75 mm rostral to the neonatal coronary suture and at a depth of 2 mm, as described previously by Glascock et al., 2011 [20]. 5 µL volumes were delivered by syringe driver (Harvard Apparatus) at a rate of 1 µL/minute. Note that the needle was left in position for around 1 minute after infusion

completion to allow pressure to dissipate and then the needle was withdrawn slowly to minimise flowback. After infusion, pups were recovered upright (in a tube holder) to encourage spinal distribution, in an incubator, for around 10 minutes before returning to the home cage and monitoring for resumption of normal maternal care.

5.3. Tissue Collection

Around 4 weeks post-injection, mice were sacrificed by an overdose of pentobarbital and a cardiac perfusion was performed with PBS. The spinal cord was then dissected *in situ*; the start of the lumbar region was identified anatomically by the end of the ribcage and presence of the lumbar enlargement. The lumbar region was fixed in 4% paraformaldehyde overnight. The remaining spinal cord was snap frozen on dry ice for viral copy number analysis. The brain was dissected and split along the midline, with the right half being fixed in 4% paraformaldehyde overnight, and left being split into regions of cortex, cerebellum and brainstem for copy number analysis. The approximate area of motor cortex cortical layer V was identified by cell size and density. The brainstem is composed of many nuclei; we quantified cells that were positive for ChAT and are likely located in the dorsal motor nucleus. Liver and heart were also snap frozen to assess off-target effects.

5.4. Immunohistochemistry

Fixed brains and lumbar spinal cord were paraffin embedded and sagittally or transversely sectioned on a microtome at 10 µm respectively. Tissue was deparaffinised and subjected to antigen retrieval in a pressure cooker (Access Revelation, pH 6.4). Sections were blocked with 5% BSA and 0.25% tx-100. Slides were then immunostained for: GFP + ChAT (motor neuron identity in spinal cord) or NeuN (neuronal identity in motor cortex region); GFP + GFAP (astrocytic identity); and GFP + Iba1 (microglial identity). Note that for double stains using ChAT, we found that staining was optimal when antibodies were added consecutively. Primary and secondary GFP staining was therefore performed and then followed by ChAT staining. For all other combinations, primary antibodies were added simultaneously in a single incubation. A summary of primary antibodies and conditions of use are shown in Table 2. Secondary antibodies used included: goat anti-chicken Alexa Fluor 488, 1:1000 (ThermoFisher, A-11039); donkey anti-chicken Alexa Fluor 488, 1:1000 (Jackson Immunoresearch, 703-545-155); goat anti-rabbit Alexa Fluor 555, 1:1000 (ThermoFisher, A27039); donkey anti-goat Alexa Fluor 555, 1:400 (Thermofisher A21432). Negative controls consisted of sections incubated in the absence of primary antibody.

Table 2: Summary of primary antibodies used for immunohistochemistry

Primary Antibody	Species / Isotype	Dilution / time / temperature	Supplier (Product code)	RRID

Anti-Green Fluorescent Protein (GFP)	Chicken Polyclonal IgY	1:1000 / Overnight / 4°C	Abcam (ab13970)	AB_300798
Anti-Choline Acetyltransferase (ChAT)	Goat Polyclonal	1:200 / 72 hour / 4°C	Merk Millipore (AB144P)	AB_2079751
Anti-Glial Fibrillary Acidic Protein (GFAP)	Rabbit Polyclonal	1:500 / Overnight / 4°C	Dako (Z0334)	AB_10013382
Anti-Ionised calcium binding adaptor molecule 1 (Iba1)	Rabbit Polyclonal IgG	1:500 / Overnight / 4°C	GeneTex (GTX100042)	AB_1240434
Anti-NeuN	Rabbit Monoclonal	1:200 / Overnight / 4°C	Cell Signalling Technology	AB_2630395

5.5. Viral DNA extraction

DNA was extracted from cortex, cerebellum, brainstem, spinal cord, liver and heart by standard phenol-chloroform extraction method. In brief, tissue was crushed with a pestle in a 1.5mL Eppendorf, and 250 µL of reporter lysis buffer (Promega) was added and tissue was crushed again. 1 µL of 20 mg/mL proteinase K was added, pulse vortexed and incubated at 50°C for 1 hour. Samples were homogenised 15x with a 21G needle. 250 µL of phenol/chloroform/isoamyl alcohol was added and vortexed vigorously for 3 minutes. Samples were centrifuged at 17000 x g at room temperature for 10 minutes. Around 225 µL of supernatant was removed to a new 1.5 mL Eppendorf and 25µL 3M sodium acetate and 1 µL glycogen was added and pulse vortex. 750 µL of 100% ethanol was added and tubes were inverted. Samples were left to precipitate overnight at -20°C. The following day, samples were centrifuged at 17000 x g at room temperature for 20 minutes. Supernatant was discarded and samples was washed with 500 µL of 70% ethanol and centrifuged at 17000 x g at room temperature for 10 minutes. Supernatant was discarded, and the sample was pulse spun, and a pipette was used to remove as much ethanol as possible. Samples were left to air dry for at least an hour at room temperature. DNA was resuspended in 25 - 50 µL of RNAse free water. Concentration and quality were determined by nanodrop and corrected to ensure that equivalent concentrations were used in qPCR. DNA was stored at -20°C.

5.6. Quantitative Polymerase Chain Reaction (qPCR)

A BioRad CFX Touch Real-Time PCR qPCR system was used to determine the number of viral genome copies present in different tissues. Primers were used that targeted the bovine growth hormone (bGH) polyA tail of the pAAV9-CMV-eGFP vector: bGH pA Forward CTCGACTGTGCCTTCTAGTTG and bGH pA Reverse CCTACTCAGACAATGCGATG. A standard plasmid (CMV.GFP plasmid clone 675.5, Vector Biolabs) was used in serial dilution to generate a standard reference curve with a known number of viral copies (see Supplementary, Fig. S.1 for curve). Copies of viral DNA were determined

using absolute quantification qPCR, with the equation $\mathbf{X_o = E_{AMP}^{(b-Cq)}}$ wherein $\mathbf{X_o}$ is copy number; $\mathbf{E_{AMP}}$ is the exponential amplification value which is 10^(-1/slope); **b** is the y-intercept of the standard curve; and **Cq** is the quantification cycle value. 1uL of DNA was used per reaction at 50ng/well as corrected after nanodrop, therefore the final $\mathbf{X_o}$ value was divided by 50, so copy number is expressed per nanogram of DNA. SYBR green was used with cycling times as shown in Table 3.

Table 3: qPCR cycling conditions for viral genome analysis

Cycling Step	Temperature	Time	Ramp rate	Number of cycles
Enzyme activation	95	5 min	2°C/sec	1
Denaturation	95	30 sec		39
Annealing/Extension	58	1 min		39
Signal Stabilisation	4	5 min		1
	90	5 min	2°C/sec	1
Hold (optional)	12	Infinite		1

5.7. Quantification and Statistical Analysis

Images of lumbar spinal cord, brainstem and motor cortex sections were taken on an Incell analyser 2200/2000 with equal exposure settings, before being taken into Image J and adjusted for brightness and contrast equally across all sections, and a flat-field correction was applied. A minimum of 3 slides per animal were used for quantification, with a minimum of 65 motor neurons per animal. Motor neurons were manually quantified for co-localisation with anti-ChAT, indicative of motor neuron identity, and anti-GFP, with the criteria that motor neurons must have a positive DAPI nuclei and express green in at least 50% of the cell within the ChAT+ boundary. For cortical anti-GFAP quantification, indicative of astrocytes, and anti-GFP quantification, Image J was used to count cells and co-localisation assessed on overlap. A manual count was then taken of GFP positive cells, to allow a correction to be applied for non-selective staining of blood vessels. Quantification of anti-ChAT and anti-GFAP, were analysed using CellProfiler™ (software available www.cellprofiler.org and we have made pipelines available where all settings and steps are fully detailed: https://github.com/CFSander/CellProfiler_astrocyte_pipelines.git) (See Supplementary Fig. S.2 for example training paradigm) [21, 22]. Investigators were blind to treatment group during all manual quantification, however blinding was not necessary for automated pipelines. Data were collated in excel and statistical analyses were undertaken in Prism10.

6. Results

6.1. AAV9 delivery to CSF leads to high motor neuron transduction in the lumbar spinal cord, with unilateral ICV delivery providing consistently high levels.

There is a distinct lack of literature that directly compares transduction levels *in vivo* in mice following different CNS-directed delivery methods of AAV9. We therefore firstly aimed to quantify the number of transduced motor neurons in the spinal cord 4 weeks after ICM, unilateral ICV or bilateral ICV repeat dose delivery of AAV9-CMV-eGFP.

We used immunohistochemical approaches (**Figure 1**) to manually count the number of motor neurons that co-localised with choline acetyltransferase (ChAT), indicating motor neuron identity, and expressed this as a percentage of the total number of motor neurons counted in the lumbar spinal cord (**Figure 2**). Note that, unexpectedly, we found cells that were quantified as positive for GFP in control animals. We are confident that this positivity is artefact, since viral genome copy number analysis in control animals was also negligible (see Table 6). We acknowledge, however, that due to artefact, it is possible that we may have overestimated transduction levels in injected animals, and the risk of false-positive identification must be highlighted. In future, it may be worth exploring alternative imaging approaches that might reduce this, although it is likely that variation in background levels will continue to present challenges. For transparency, we have included control data (as opposed to expressing levels relative to control), to highlight the challenges with eliminating background staining with GFP immunohistochemistry. We noted that GFP fluorescence intensity appeared visually higher in the bilateral repeat dose ICV group compared to other methods, but due to background variation, quantification was challenging. All tissue was fixed and treated identically as far as possible and controls with primary antibody excluded were included (Supplementary, Fig. S.4), with antibody non-specificity and autofluorescence being the likely the origin of such background.

We found that all delivery methods lead to high levels of motor neuron transduction in the spinal cord, with over 68% of lumbar motor neurons being transduced in all groups, as summarised in Table 4. We noted that unilateral ICV approaches yielded more consistent, higher percentages of transduced motor neurons in the lumbar spinal cord than other approaches (**Figure 2**). Note that, as expected, and consistent with previous reports [23, 24], intramuscular delivery failed to show retrograde transduction of motor neurons in the spinal cord (Supplementary, Fig. S.3).

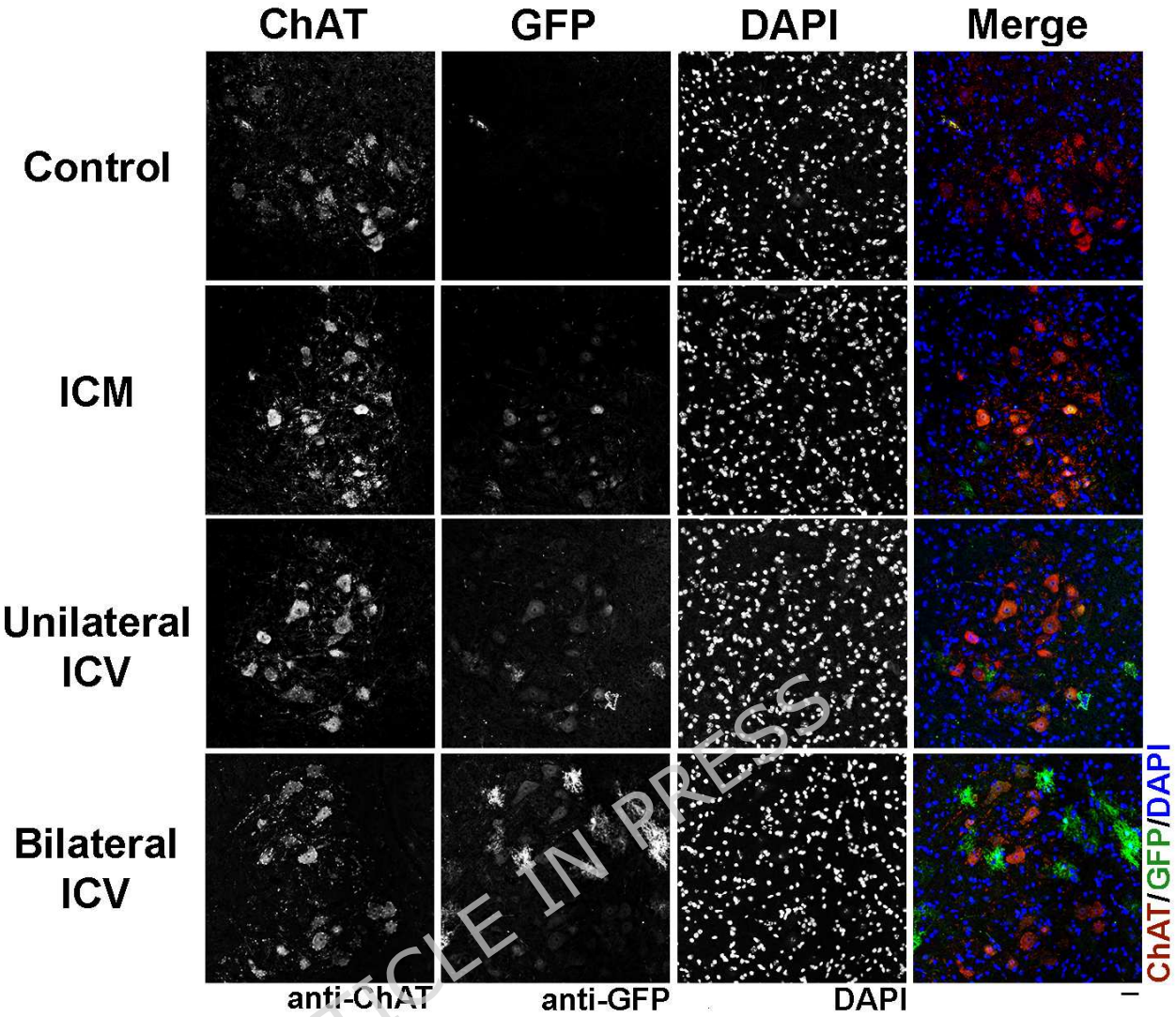

Figure 1: Visualisation of choline acetyltransferase (ChAT) positive cells, indicating motor neurons, and GFP co-localisation in the ventral horn of the lumbar spinal cord in mice around 4 weeks after AAV9-CMV-eGFP delivery. *Note that transduction can be clearly visualised in all delivery conditions. Note that there are transduced cell types particularly visible in the bilateral repeat dose ICV condition which are not motor neurons and which are likely astrocytes. Differences in visible motor neuron numbers reflect differences in field selection, rather than biology. Sections labelled with anti-ChAT, anti-GFP and DAPI. Scale bar = 40 µm.*

Table 4: MN counts in lumbar spinal cord and average transduction level

Route of Administration	Total MNs counted (ChAT+)	Transduced MNs (eGFP+/ChAT+)	Percentage of Transduced MNs ±SEM (%)
ICM (n=5)	661	452	68.4 ± 11
Unilateral ICV (n=5)	744	662	89.0 ± 3
Bilateral repeat dose ICV (n=4)	643	482	75.0 ± 9

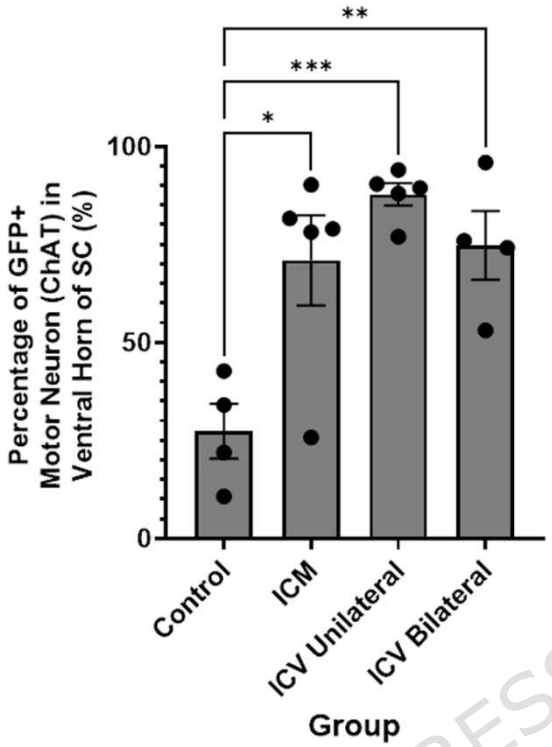

Figure 2: Quantification of the percentage of GFP positive cells that are co-localised with ChAT, indicating transduced motor neurons, in the spinal cord after different CNS-directed delivery methods of AAV9-CMV-eGFP. *Note that there are high levels of transduction in all groups, however the most consistent and highest transduction is seen after unilateral ICV delivery. ICM = intra-cisterna magna; ICV unilateral = unilateral intra-cerebroventricular; ICV bilateral = bilateral intra-cerebroventricular delivery repeated dose group. One-way ANOVA with Tukey's correction for multiple comparisons. *p≤0.05, **p≤0.01 ***p≤0.001. Error bars = mean ± SEM.*

6.2. AAV9 delivery to CSF leads to high motor neuron transduction in the brainstem but not in the motor cortex

We next sought to investigate and compare the extent to which motor neurons in the brainstem and cortex were targeted by ICM and ICV delivery methods of AAV9-CMV-eGFP.

Using immunohistochemistry (**Figure 3**), we manually quantified the co-localisation between ChAT, indicative of motor neurons, and GFP, indicating positive transduction in the brainstem and expressed the number of co-localised motor neurons as a percentage of total motor neurons counted (**Figure 4**).

We found that motor neuron transduction was high in the brainstem in both conditions, with >55% of motor neurons transduced in all groups, as summarised in Table 5, however we noted high variability (**Figure 4**).

In the cortex, however, we were unable to detect co-localisation of the neuronal marker (anti-NeuN) with GFP, suggesting minimal neuronal transduction (**Figure 5**).

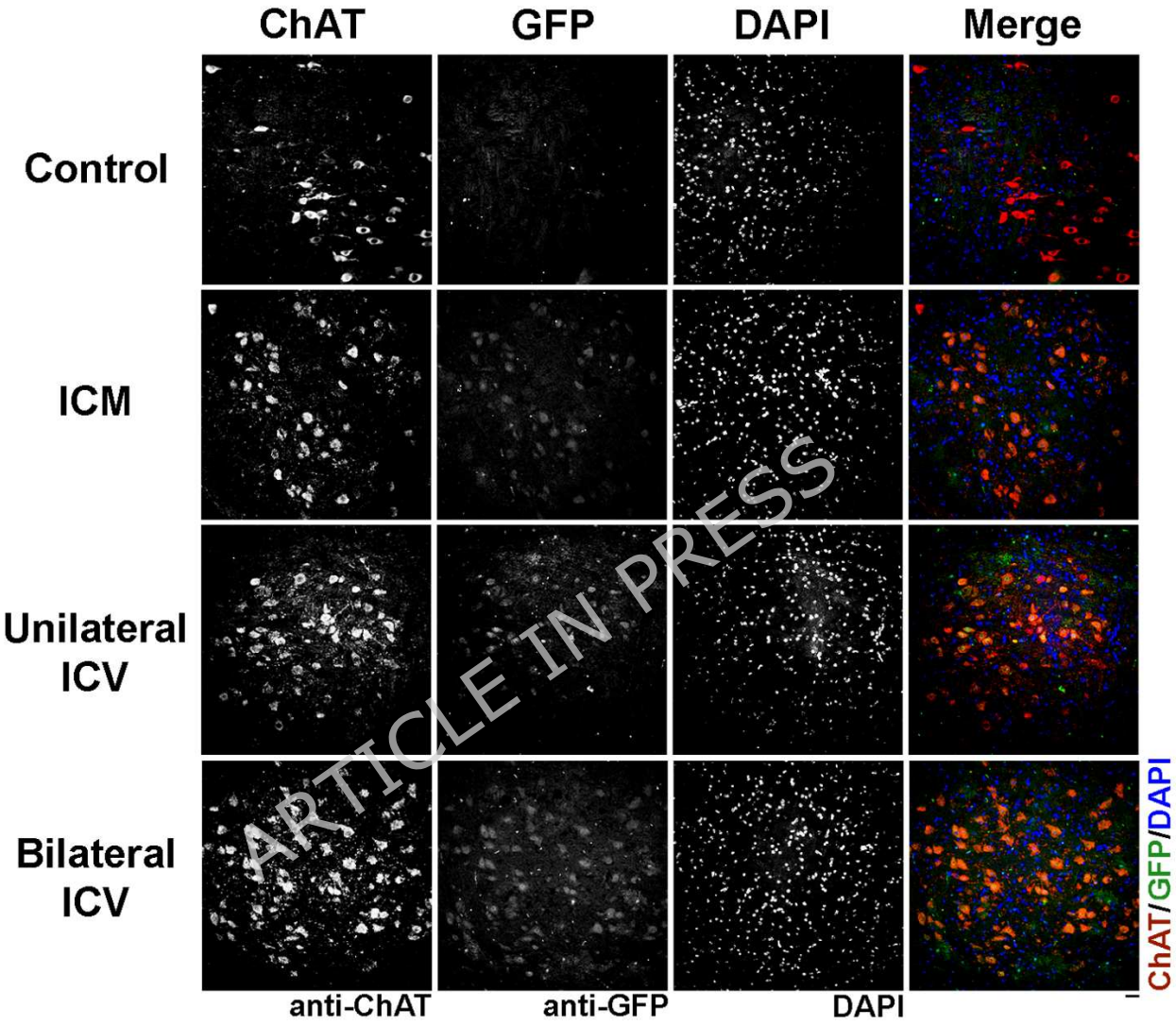

Figure 3: Visualisation of choline acetyltransferase (ChAT) positive cells, indicating motor neurons, and GFP co-localisation in the brainstem in mice around 4 weeks after AAV9-CMV-eGFP delivery. *Note that transduction can be clearly seen in all delivery conditions. Sections are labelled with anti-ChAT, anti-GFP and DAPI. Scale bar = 20 µm.*

Table 5: MN counts in brainstem and average transduction level

Route of Administration	Total MNs counted (ChAT+)	Transduced MNs (eGFP+/ChAT+)	Percentage of Transduced MNs ± SEM (%)
ICM (n=5)	473	262	55.4 ± 15
Unilateral ICV (n=5)	424	296	69.8 ± 16

Bilateral ICV Repeat Dose (n=4)	850	601	70.7 ± 16

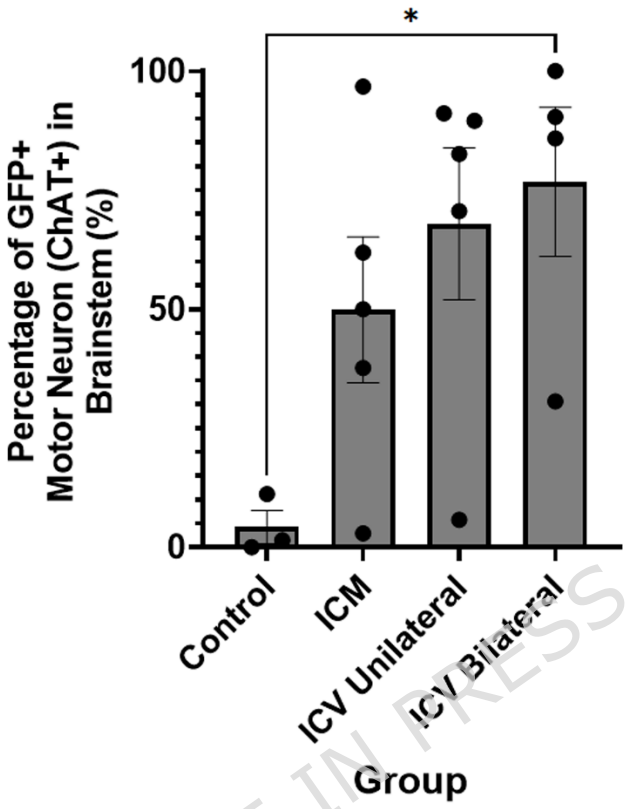

Figure 4: Quantification of the percentage of GFP positive cells that are co-localised with ChAT, indicating transduced motor neurons, in the brainstem after different CNS-directed delivery methods of AAV9-CMV-eGFP. *Note that there are high levels of transduction in all groups, although this is variable between animals. ICM = intra-cisterna magna; ICV unilateral = unilateral intra-cerebroventricular; ICV bilateral = bilateral intra-cerebroventricular repeat dose delivery. One-way ANOVA with Tukey's correction for multiple comparisons. *p≤0.05. Error bars = mean ± SEM.*

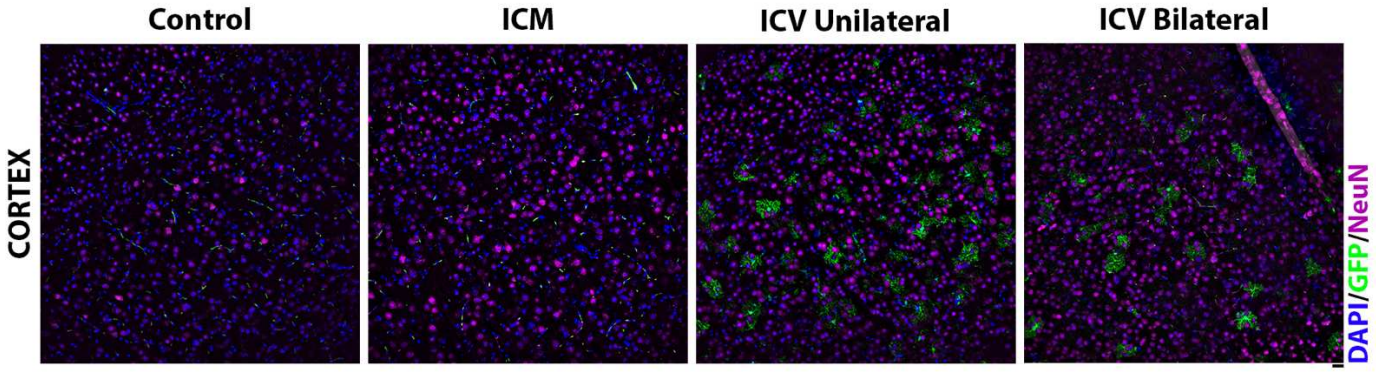

Figure 5: Visualisation of the neuronal marker, anti-NeuN, and GFP in the motor cortex in mice around 4 weeks after ICV AAV9-CMV-

eGFP delivery. Note that a lack of co-localisation is seen with NeuN, suggesting minimal neuronal transduction. Note that we can see other non-neuronal cell types that are transduced following ICV administration in the cortex. An example of region of interest selection at lower magnification is provided in supplementary material (Fig. S.5). Scale = 20μm.

6.3. The number of viral genome copies in spinal cord and brainstem is higher with ICV delivery methods.

Quantification of viral genome copy number can provide additional insight into the biodistribution and transduction efficiency of gene therapy vectors. Here, we used quantitative PCR (qPCR) on vector genome DNA isolated from various CNS tissues to gain further insight into viral distribution and compare this across delivery methods. We quantified the average number of vector genome copies/ng of DNA in each tissue (Table 6 and Figure 6) by extrapolating Ct values from a standard curve generated from a GFP plasmid with known viral copy number (see Supplementary data, Fig. S.1). As expected, we found that the control group had negligible viral copy numbers, confirming that our detection method was specific, and further evidencing that immunohistochemical positivity previously detected in control is artefact.

We were able to detect viral copies in all treatment groups. There was a trend towards a higher viral copy number in spinal cord and brainstem after ICV delivery methods.

In spinal cord, there were between 7-8 copies/ng of DNA after ICM delivery, threefold higher following unilateral ICV at around 30 copies/ng of DNA and significantly higher after bilateral repeat dose ICV at around 308 copies/ng of DNA, as summarised in Table 6 and Figure 6. The viral genome copy number does not necessarily align with data obtained for motor neuron transduction rates obtained from immunohistochemical analysis (Figures 2 and 4). We can attribute this to either transduction of other cell types, such as astrocytes, or perhaps there is a limit to transduction efficiency such that higher viral genome copy number does not translate to a greater transduction rate. It is also possible that overexpression of GFP protein could lead to immunogenicity which could interfere with, and paradoxically, reduce GFP expression. At this age although unlikely, others have indicated that neutralising antibodies may be present within 24 hours of first dose, thus cannot be excluded [25].

A similar trend was also seen in brainstem, with around 9 copies/ng of DNA after ICM, 464 copies/ng of DNA after ICV unilateral and 1053 copies/ng of DNA after bilateral repeat dose ICV, also summarised in Table 6 and Figure 6. We noted increased variability in viral copy number at higher levels. In cortex, we observed high viral genome copy numbers following ICV delivery, despite a lack of neuronal transduction. Taking copy number results together with immunohistochemical assessment, this is likely due to the

high level of astrocyte transduction in cortex (see Results, Table 7 and Fig. 7).

Table 6: Viral copy number analysis in central tissues as determined by qPCR.

Tissue	Number of viral copies/ng of DNA (Mean ± SEM)			
	Control (n=4)	**ICM (n=5)**	**Unilateral ICV (n=3-5)**	**Bilateral ICV Repeat Dose (n=4-5)**
Spinal cord	0	7.7 ± 2	30.1 ± 17	308.9 ± 55
Brainstem	0	9.1 ± 3	463.5 ± 148	1053.0 ± 200
Cerebellum	0	65.4 ± 40	6.9 ± 3	46.5 ± 17
Cortex	0	56.9 ± 54	5598.0 ± 3688	3432.0 ± 1101

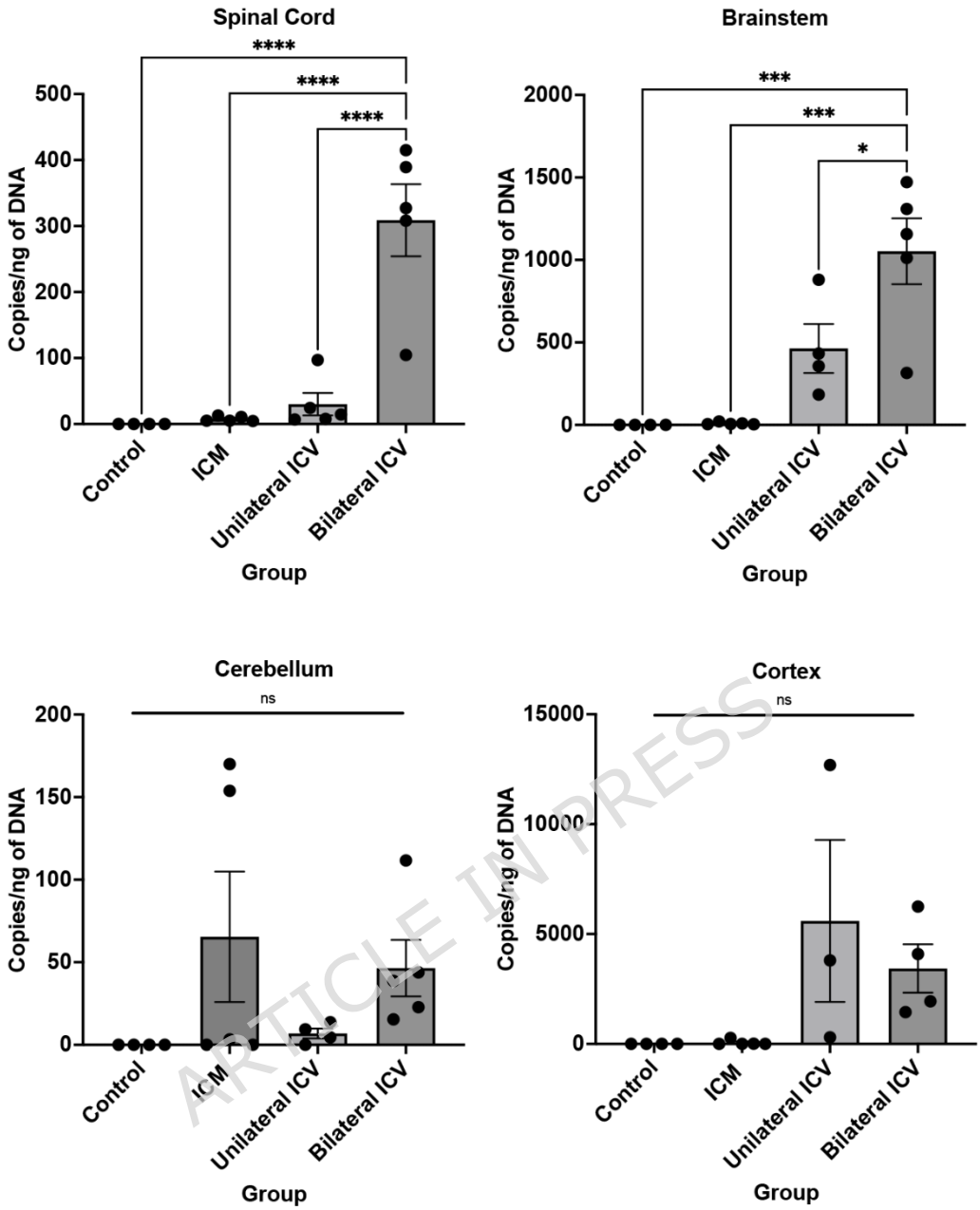

Figure 6: Quantification of viral copy number in spinal cord, brainstem, cerebellum and cortex. *Quantitative PCR on CNS tissue suggests that there are high copy numbers in spinal cord and brainstem, with a trend towards higher copy number in these tissues when delivered intra-cerebroventricularly (ICV). ICM = intra-cisterna magna; ICV unilateral = unilateral intra-cerebroventricular; ICV bilateral = bilateral intra-cerebroventricular repeat dose delivery. One-way ANOVA with Tukey's correction for multiple comparisons. ns=not significant, *p≤0.05, ***p≤0.001, ****p≤0.0001. Error bars = mean ± SEM.*

6.4. ICV delivery of AAV9-CMV-eGFP results in significantly higher astrocytic transduction than other delivery methods, particularly in cortex

In this work, we intended to selectively target motor neurons, however, it was evident from immunohistochemistry that other cell types had been transduced after AAV9-CMV-eGFP delivery that were not ChAT- or NeuN-positive. Using immunohistochemistry, we identified these cells as being positive for the astrocytic marker, glial fibrillary acidic protein (GFAP), in spinal cord, brainstem and cortex (**Figure 8**, **Figure 9** and **Figure 10** respectively). In cortex, cells also appeared negative for the microglial marker, anti-ionised calcium binding adaptor molecule 1, Iba1 (**Figure 11**), indicating that these cells were likely astrocytic in identity.

We quantified the number of GFP positive cells that co-localised with GFAP and expressed this as a percentage of the total number of GFAP positive cells. As summarised in Table 7, we found that there were significantly higher percentages of astrocytes transduced with a Bilateral ICV repeat dose approach in spinal cord and, particularly in the cortex. Astrocytic transduction was minimal with ICM delivery in all regions. In ICV groups, we found significantly more astrocytic transduction in spinal cord and brainstem.

In the bilateral ICV repeat dose group, in spinal cord, we found around 1.4% of astrocytes were transduced, and in brainstem 0.37% of astrocytes were transduced (Table 7, **Figure 7**).

Overall, we found that ICV delivery resulted in significantly higher astrocytic transduction than ICM delivery, although it is worth noting that numbers were low in spinal cord and brainstem, but high in cortex (Table 7, **Figure 7**). Further work is required to determine the biological significance of this, and to assess routes for better targeting of upper motor neurons.

Table 7: Percentage of transduced astrocytes in spinal cord, brainstem and cortex.

Tissue	Percentage of transduced astrocytes (Mean ± SEM)			
	Control (n≥2)	ICM (n≥3)	Unilateral ICV (n≥4)	Bilateral ICV Repeat Dose (n≥3)
Spinal Cord	0.04	0.10 ± 0.07	0.31 ± 0.14	1.42 ± 0.32
Brainstem	0.07 ± 0.03	0.05 ± 0.02	0.04 ± 0.03	0.37 ± 0.04
Cortex	0 ± 0	0.50 ± 0.50	16.20 ± 4.31	25.60 ± 9.50

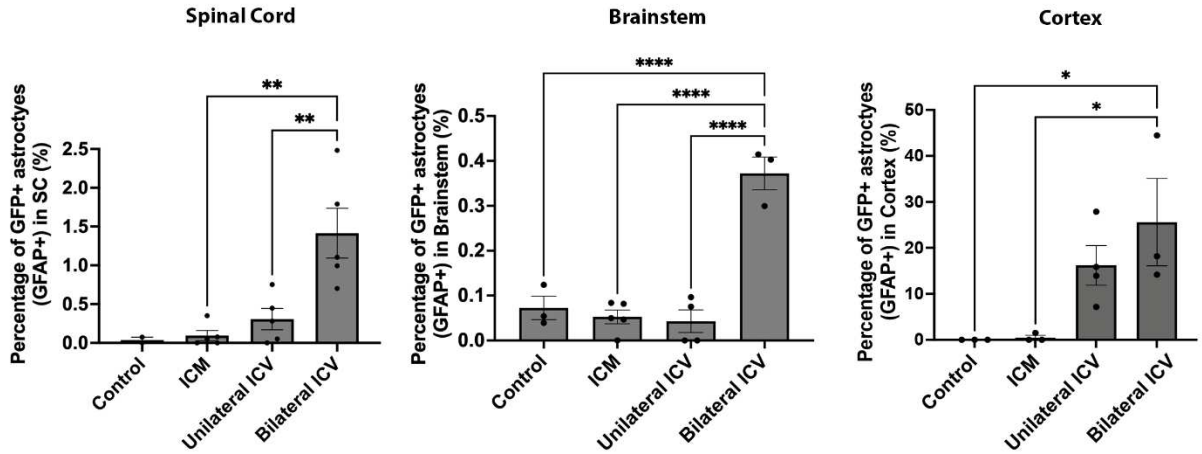

Figure 7: Quantification of the percentage of transduced astrocytes in spinal cord, brainstem and cortex. *Quantification of GFP positive cells that co-localised with the astrocytic marker, GFAP, showed that percentages of transduced astrocytes following intra-cisternal magna (ICM) and unilateral intra-cerebroventricular (ICV) injection are not significantly different than control, suggesting minimal astrocytic transduction in these groups. Note that there are a small but significantly higher percentage of transduced astrocytes following bilateral ICV repeat dose delivery in spinal cord and brainstem. Note that in cortex, ICV delivery appears to target a much higher percentage of astrocytes, compared to ICM. One-way ANOVA with Tukey's correction for multiple comparisons. *p≤0.05, **p≤0.01, **** p≤0.0001 Error bars = mean ± SEM.*

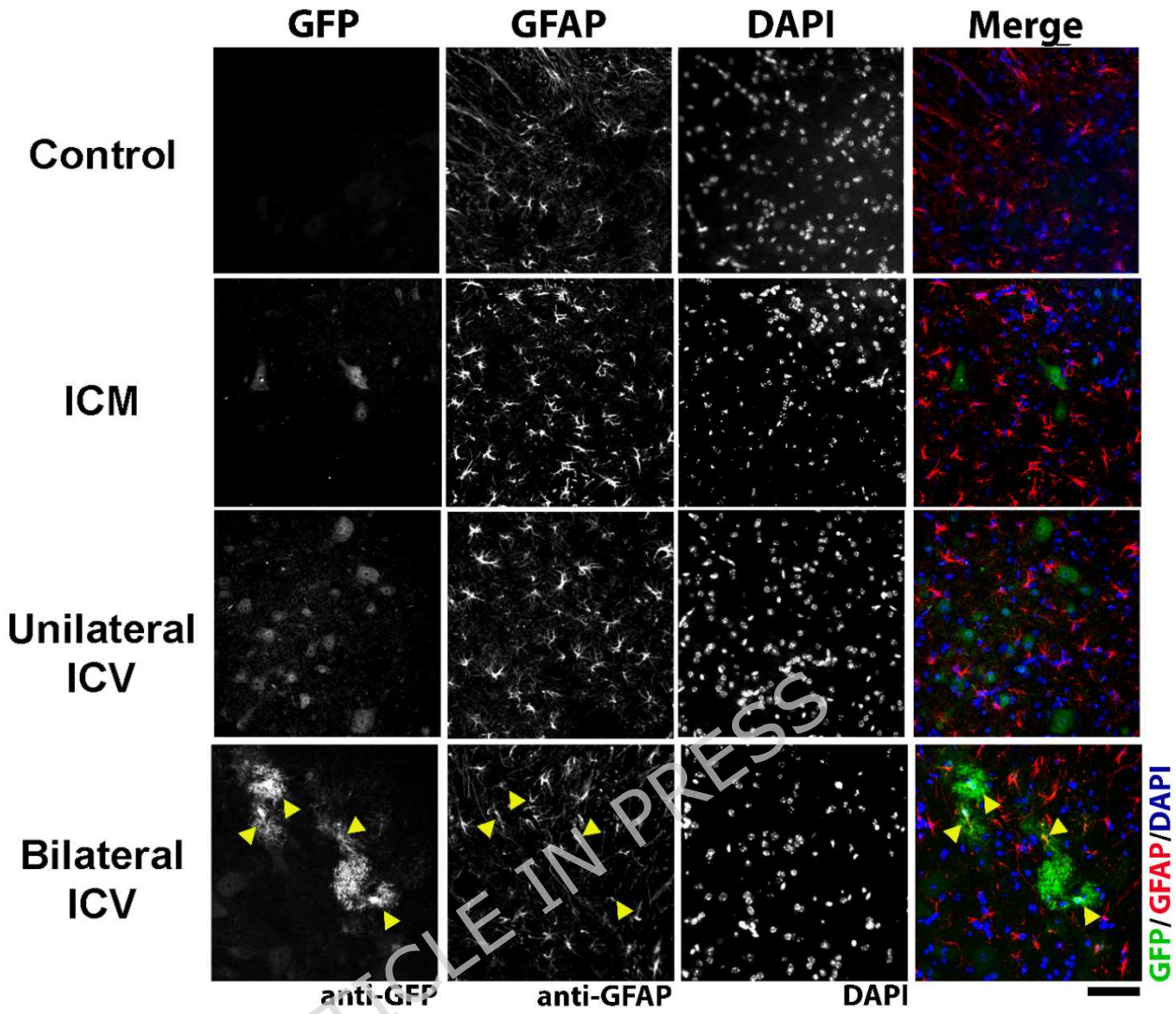

Figure 8: Visualisation of glial fibrillary acidic protein (GFAP) positive cells, indicating astrocytes, and GFP co-localisation in the spinal cord in mice around 4 weeks post AAV9-CMV-eGFP delivery. *Note that transduction of astrocytes can be clearly seen in bilateral ICV repeat dose conditions (examples indicated by yellow arrowheads). Sections are labelled with anti-GFP, anti-GFAP and DAPI. Scale bar = 50 µm.*

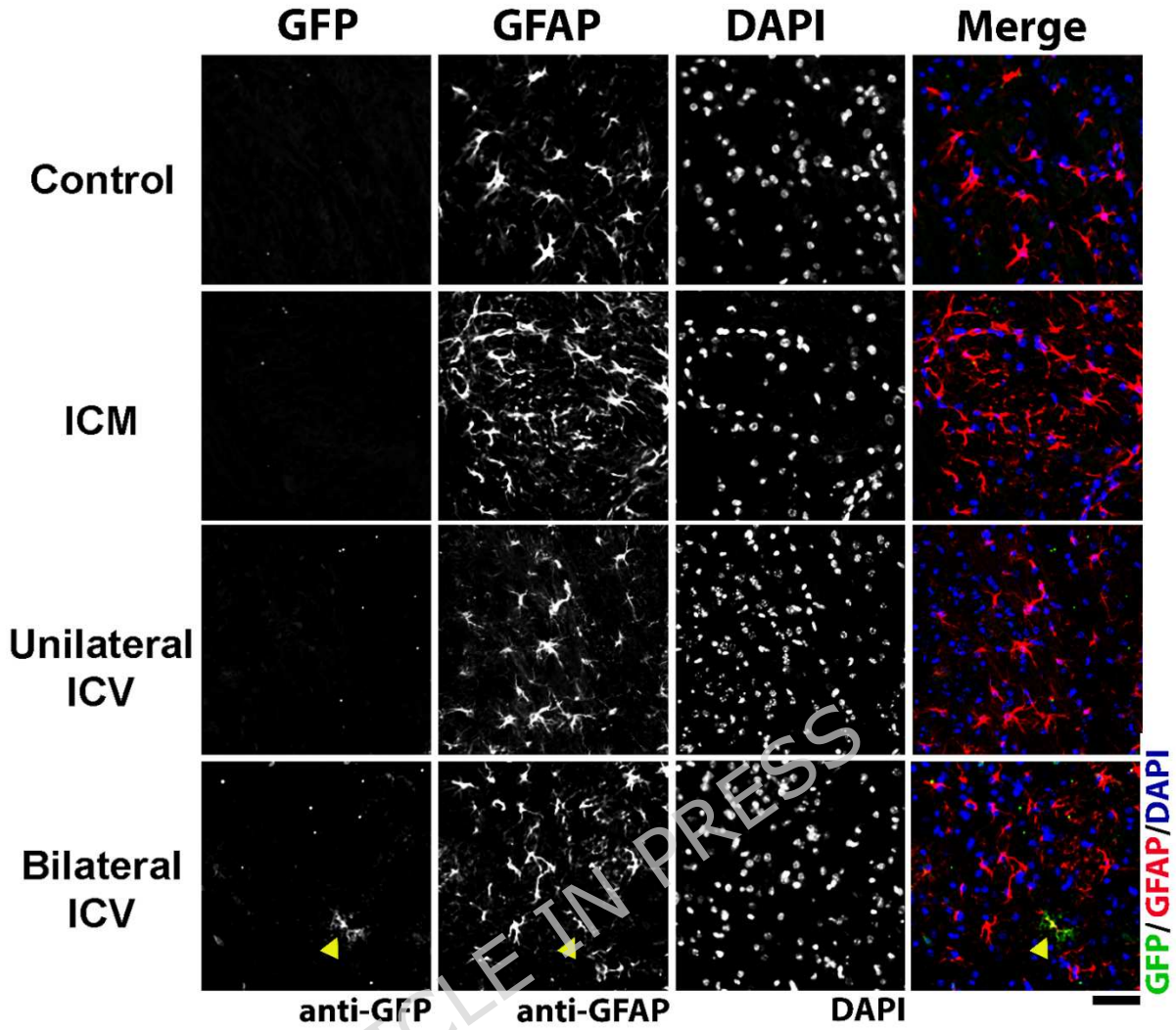

Figure 9: Visualisation of glial fibrillary acidic protein (GFAP) positive cells, indicating astrocytes, and GFP co-localisation in the brainstem in mice around 4 weeks post AAV9-CMV-eGFP delivery. *Note that transduction of astrocytes can be clearly seen in bilateral ICV repeat dose group (example indicated by yellow arrowhead). Sections are labelled with anti-GFP, anti-GFAP and DAPI. Scale bar = 50 µm.*

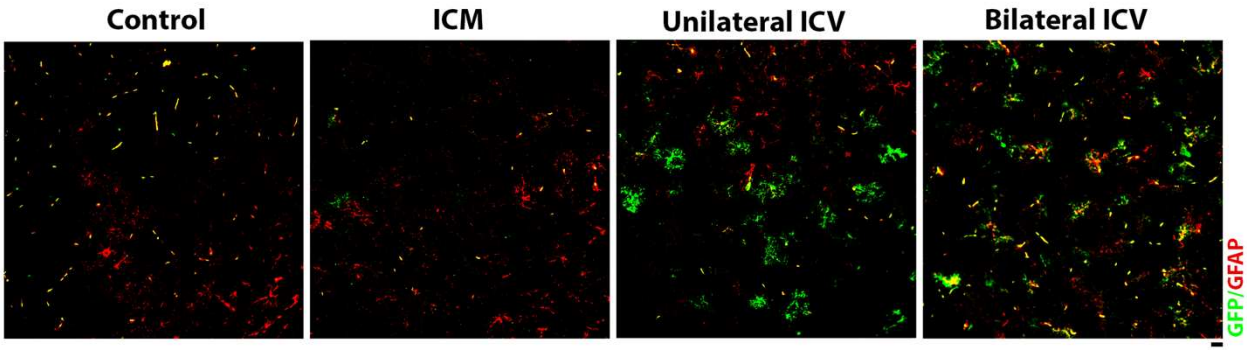

Figure 10: Visualisation of glial fibrillary acidic protein (GFAP) positive cells, indicating astrocytes, and GFP co-localisation in the cortex in mice around 4 weeks post AAV9-CMV-eGFP delivery. *Note that transduction of astrocytes can be clearly seen in both ICV groups. Sections are labelled with anti-GFP, anti-GFAP and DAPI. Scale bar = 20 µm.*

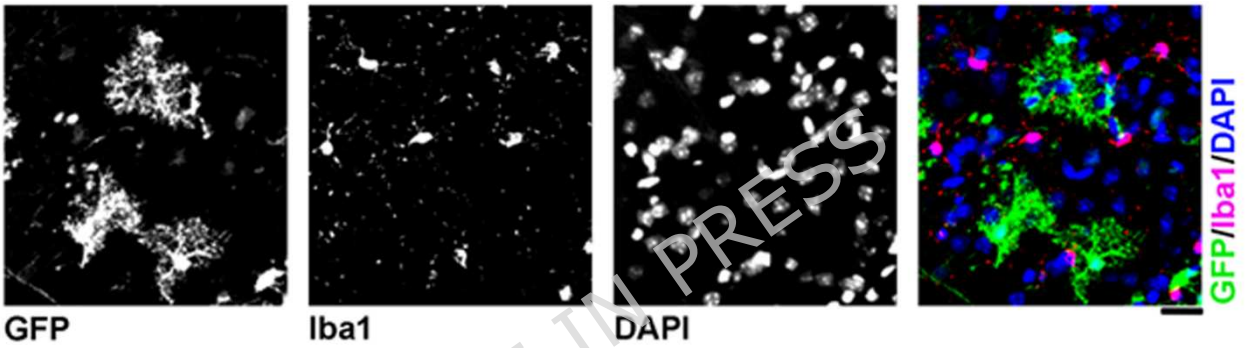

Figure 11: Micrograph showing a lack of GFP co-localisation with the microglial marker in cortex, anti-ionised calcium binding adaptor molecule 1, Iba1. *No overlap between GFP and Iba1 was seen. Sections are labelled with anti-GFP, anti-Iba1 and DAPI. Scale bar = 20 µm.*

6.5. Unilateral ICV delivery of AAV9-CMV-eGFP provides the lowest levels of peripheral transduction

With AAV-mediated gene therapies, there is concern regarding peripheral, off-target effects, particularly pertaining to hepatotoxicity. We therefore quantified the number of viral genome copies found in liver and heart, to quantify the peripheral viral load following different CNS-directed delivery methods.

As summarised in Table 8 and Figure 12, after ICM administration there were around 9 and 14 copies/ng in the liver and heart respectively. Unilateral ICV delivery resulted in the lowest and most consistent number of copies, with <3 copies/ng of DNA in liver and heart. As might be expected with a higher dose, bilateral ICV repeat dose resulted in significantly more viral copies than any other delivery route, with around 35 and 23 copies/ng

of DNA in liver and heart respectively, although we did not see any overt signs of toxicity in study animals. When considering the best route of administration for motor neuron targeting, it is worth noting that a bilateral repeat dose approach could lead to 10x more viral load in the liver than another delivery method, despite achieving similar levels of motor neuron transduction in spinal cord and brainstem. Overall, achieving a balance between specific transduction in the CNS versus off-target effects is a critical consideration.

Table 8: Viral copy number analysis in peripheral organs as determined by qPCR.

Tissue	Number of viral copies/ng of DNA (Mean ± SEM)			
	Control (n=4)	ICM (n=5)	Unilateral ICV (n=5)	Bilateral ICV Repeat Dose (n≥4)
Liver	0	9.0 ± 4	2.8 ± 2	35.1 ± 13
Heart	0	13.7 ± 7	2.2 ± 2	23.3 ±13

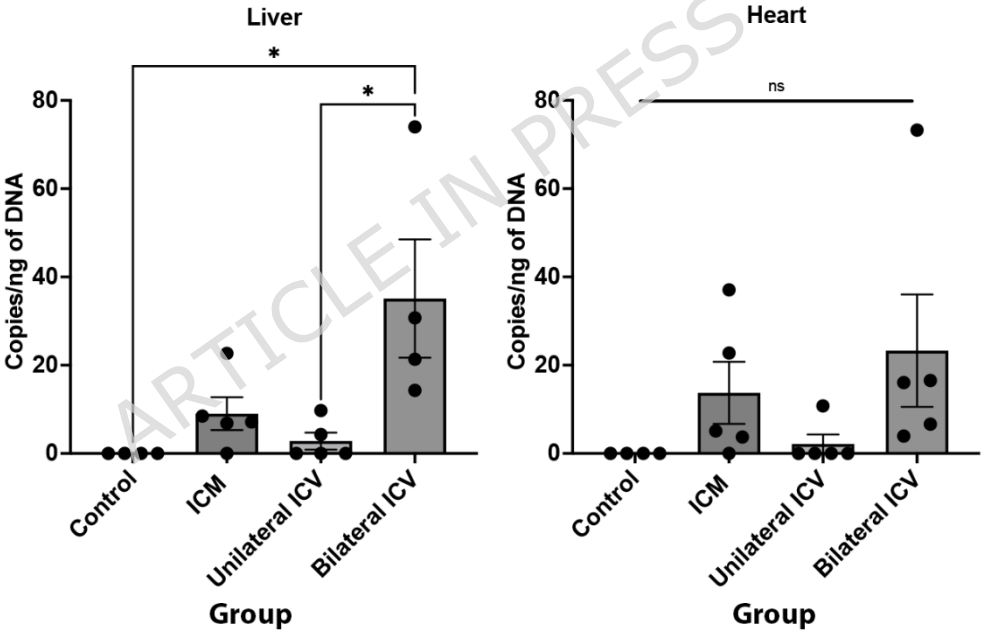

Figure 12: Quantification of viral copy number in liver and heart. *qPCR on peripheral tissue suggests that there is limited off-target transduction in peripheral organs. Note that Unilateral ICV achieves the lowest and most consistent number of viral copies in liver and heart. Also note that Bilateral ICV repeat dose delivery results in significantly more viral copies in the liver. One-way ANOVA with Tukey's correction for multiple comparisons. ns=not significant, *p≤0.05. Error bars = mean ± SEM.*

7. Discussion

In line with previous studies, we have demonstrated that CNS-directed delivery of scAAV9-CMV-eGFP in neonatal mice can transduce motor neurons to high levels. We found that unilateral ICV delivery of scAAV9-CMV-eGFP transduced over 88% of motor neurons in the lumbar spinal cord and over 69% of motor neurons in brainstem. More generally, at 4 weeks post-injection, we found that any CNS-directed route transduced over 68% of motor neurons in the lumbar spinal cord and over 55% of motor neurons in the brainstem. We have highlighted challenges with GFP immunohistochemistry which must be taken into consideration, since staining artefact may lead to an overestimation of transduction levels. We therefore must be cautious when comparing transduction levels reported here to other studies since most studies fail to quantify or do not report control artefact levels. Greater transparency of potential false-positive levels is required in the literature, and we hope that our work highlights challenges with what might be assumed to be simple visualisation of a fluorescent protein. Viral copy numbers in the CNS were also high across all groups, however we noted that bilateral ICV repeat dose delivery, whereby the titre is effectively doubled across two days, resulted in significantly higher viral copies in the liver. We also noted that bilateral ICV repeat dosing leads to significantly more astrocytic transduction in spinal cord (around 1.4%) and brainstem (around 0.37%) than other delivery methods, although numbers remained low. In cortex, either unilateral or bilateral ICV approaches transduced significantly more astrocytes (>16%), compared to the ICM group, where astrocytic transduction was almost negligible.

Taking motor neuron transduction levels and viral copy number data together, unilateral ICV delivery may provide the best balance between achieving high and consistent lower motor neuron transduction whilst minimising peripheral effects. If astrocytic transduction is desired, then ICV approaches could be effective, but titre should be optimised to determine potential dosing thresholds that lead to astrocytic transduction with minimal peripheral impact. If avoiding astrocytic targeting, then an ICM approach may be more appropriate. Systemic delivery should also be considered if non-neuronal subtypes are the intended target, as the literature suggests that more widespread targeting of periphery and other cell types [4, 24, 26-29]. Further work is required to optimise targeting of upper motor neurons with these methodologies.

7.1. Systemic versus CNS-directed delivery of AAV9

Vascular delivery of AAV9 remains the most widely adopted infusion route and is also more applicable to paediatric patients. Whilst an intravascular approach has proven clinical potential and application, challenges remain. The most obvious challenge lies in the large quantities of vector that are required to achieve significant CNS-targeting. Only a fraction of the vector penetrates the blood brain barrier (BBB), thus making widespread CNS delivery historically challenging [2, 4], although development of BBB-penetrant capsids has been ongoing and several recent BBB-penetrating

AAV9 capsid variants have been engineered that show widespread CNS transduction [30-33]. With an intravenous approach using scAAV9-CBh-GFP in neonatal mice, Foust et al., 2009 reported one of the highest levels seen with a systemic approach, reporting up to 61% motor neuron transduction in mice. However, vascular delivery also leads to widespread targeting of astrocytes throughout the spinal cord and brain, and, most notably, in peripheral organs [4, 24]. Similar peripheral organ targeting, and astrocytic transduction in mice are reported with AAV9 after systemic delivery throughout the literature [3, 4, 26-29]. Whilst targeting of astrocytes may not necessarily be undesirable, as there is potential for astrocytes to deliver secreted transgene products to the CNS, the additional challenges of toxicity, immunogenicity and circulating antibodies with such large infusion volumes are problematic.

With systemic delivery approaches, large vector doses are required to reach the CNS due to full-body distribution. Increasing the viral load consequently increases peripheral organ exposure. Indeed, significant concerns over liver toxicity have emerged in both clinical and non-clinical settings in spinal muscular atrophy, Duchenne muscular dystrophy and myotubular myopathy [34-39].The liver is highly vascularised, receiving around 25% of cardiac output and around 30% of the body's total volume per minute [40, 41], which may drive hepatic tropism. The mechanisms by which the liver tolerates, or fails to tolerate, AAV9 have been reviewed recently [42], however in brief transduction of AAV vector in macrophages in the liver, known as Kupffer cells, are thought to elicit an immune response and subsequently eliminate the therapeutic effect of delivered therapies by developing antibodies to the capsid, transgene, or through cytotoxic T-cell-mediated mechanisms. Activation of capsid-specific T cells may result in destruction of transduced hepatocytes and result in consequent hepatotoxicity. Acute liver injury has been found to correlate with high hepatocellular load, macrophage activation, and type 1 interferon innate virus-sensing pathway responses [34]. Thus, reducing the viral load, as can be achieved with CNS-directed AAV9 delivery, has clear advantages, despite being more invasive and technically challenging. The presence of anti-AAV antibodies in the bloodstream, even at low titres, can block transduction of tissues by intravenous AAV9 [4]. Anti-AAV antibodies are common in human and non-human primates, although normally lower in infants and young children [10, 43, 44].

Since reduced doses of vector are required to reach clinically relevant transgene expression with CNS-directed delivery, the immunogenicity risk is inherently lower. Work in nonhuman primates, suggests that direct CSF delivery can yield widespread transduction with a dose ten times lower than intravenous delivery [45]. Thus, CNS-directed approaches offer a compelling alterative. Our data indicate that unilateral ICV delivery results in minimal viral genome copies in the liver, which is promising from a toxicity perspective. Notably, bilateral ICV delivery with an increased titre via repeated dosing resulted in significantly higher viral load in the liver, however toxicity was not expected or observed with this viral load. Our

observations may be due to increased titre of the vector, since we doubled the dose with a bilateral approach, however we cannot rule out other mechanisms of augmentation, which we will discuss. We must also note that here, effects of repeated dosing versus higher titre cannot be distinguished, and that delivering bilaterally within the same session would help to elucidate this. ICV delivery is already used in clinical trials such as those in Canavan disease (NCT04833907) and mucopolysaccharidosis type II (NCT04571970) and so is already clinically translatable. In non-human primates, ICV delivery has been shown to transduce over 65% of motor neurons in the lumbar spinal cord at 3 weeks post-delivery, and ICM has been shown to transduce neurons in the brain [46, 47]. Due to the close anatomical relationship between brainstem and the cisternal space, ICM routes of delivery carry higher procedural risk. In the clinic, an intrathecal catheter via the subarachnoid space from a lumbar puncture may reduce invasiveness of an ICM procedure; in non-human primates, delivery to the lateral ventricle or ICM with a catheter has been shown to effectively target cervical motor neurons [48]. Work using AAV9-mediated gene delivery in a mouse model of mucopolysacccharidosis type I examined the therapeutic effectiveness of different routes of CSF delivery and found that all treated animals were indistinguishable from control, regardless of route [49]. Our data agrees and suggests that the main consideration when choosing between routes in murine preclinical work likely resides in desire to achieve astrocytic transduction. ICV appears to result in higher and more consistent lumbar motor neuron transduction, however, higher numbers of astrocytes are transduced, especially in cortex. If seeking to avoid astrocytic transduction, ICM may be a better option.

It is important to note that delivery of AAV9 into CSF directly does not negate the challenge of circulating pre-existing anti-AAV antibodies [10], and mild dorsal root ganglion toxicity has been highlighted in preclinical animal studies [38], however only one case has been reported in humans [50]. Since transduction can be achieved at lower viral titre within the CNS compartment, immunogenicity risks are reduced. Studies in dogs have reported similar transduction levels regardless of route (ICV or ICM), however animals receiving ICV have been reported to develop encephalitis associated with a T cell response, which did not present after ICM delivery [51]. Immune tolerance of AAV-based therapies, screening for neutralising antibodies and immunosuppression remain important clinical considerations. Here, we did not pre-screen for neutralising antibodies due to the very young age of delivery, however it is possible that repeat could lead to development of neutralising antibodies - which has been shown to develop within one day in mice [25] - that may interfere with transduction or lead to more inflammatory processes and damage. In addition, intra-CSF delivery of AAVs has been shown to induce more dorsal root ganglion (DRG) pathology in non-human primates than if AAV is delivered intravenously [52]. We did not assess DRG biodistribution here, however including this in future may allow us to better understand and predict the consequences of DRG transduction.

Note that we trialled intramuscular delivery of vector into gastrocnemius muscle in neonatal and adult mice, however, despite evidence of myofiber transduction, there was minimal evidence of retrograde transduction to motor neurons in the lumbar spinal cord (see Supplementary Fig. S.3). Previous studies have similarly shown that there is minimal transduction to lumbar spinal cord after direct intramuscular hindlimb delivery of AAV9 [23, 24]. This route of administration could be useful if seeking to selectively target peripheral muscle but does not appear useful for targeting alpha-motor neuron somata. It would be interesting to assess alternative approaches for evaluating CNS biodistribution. Co-injection of the same AAV serotype by two different routes with different reporters for each route of administration, for example, may provide an interesting way to compare distribution within the same animal. However, consideration of tolerable volumes, system pressure and distribution to other cell types, and visualisation of co-stains, would likely be pertinent. Assessing if both CSF-delivery methods remain equally as effective if vectors are delivered to mice during adulthood would be interesting, since age-dependent declines in transduction have been described with CNS-directed therapies [53]. We chose to administer at neonatal stages as this is the major timepoint used in studies for therapeutic proof of concept and particularly where neurodegenerative phenotypes develop rapidly [15].

Another critical consideration is that here, we failed to find evidence of motor neuron transduction in the motor cortex. There could be several reasons for this linked into dose, route, age at time of delivery, and viral vector identity that merit further work. This is undoubtedly a key consideration for gene therapy work in diseases such as ALS, since both upper and lower motor neurons are affected. Previous work has reported expression in brain using AAV9, although transduction in motor cortex appears low; notably however, identity is not clearly defined, thus the possibility that positivity arises from e.g. transduced astrocytes, cannot be excluded [54]. In future work, it would be pertinent to assess other spinal cord regions to gain broader insight into vector distribution. Here, we chose to use a CMV promoter to drive expression, which expresses ubiquitously but has been described as exhibiting neuron-predominant expression with AAV9 when delivered to CSF in non-human primates at lower titres [55]. Our data is largely in line with this, as we saw astrocytic transduction with a repeated dose in the bilateral ICV group. Assessing alternative promoters with greater neuronal specificity (e.g. synapsin 1, CaMKIIα or Hb9 or ChAT for motor neurons) would be interesting. For example, work using synapsin promoter-driven recombinant AAV9 in neonatal mice has shown that direct CSF delivery can specifically target neurons in motor cortex, spinal cord, peripheral nerves and ganglia [56]. Our work highlights the importance of assessing and optimising viral distribution for preclinical work, to ensure vectors are reaching their intended target to ensure that they are assessed for true therapeutic efficacy.

7.2. Augmentation of transduction with consecutive delivery of AAV9

To achieve our highest titre group, we delivered vector across two sessions on consecutive days. The reasoning for this was primarily driven by our aim to increase vector titre within the constraints of the injection volume, to limit the risk of increasing intracranial pressure, whilst keeping the construct constant. At 4 weeks post-injection, we anticipated strong expression of the transgene [14]. Fortuitously, our repeat dosing regimen led to an interesting observation: when scAAV9-CMV-eGFP was delivered bilaterally across two days, effectively doubling viral titre, we noted that there was a significant increase in viral copy number in spinal cord and brainstem above the two-fold level that we might have anticipated. The mechanisms underpinning such an increase in viral vector load remain unclear. Whilst we will suggest some explanations for this here, we must recognise that there are limitations since effects of repeated dosing versus higher titre delivery cannot be distinguished here.

The CNS is described as an immune-privileged compartment, which likely serves to preserve tissues with limited regenerative capacity from destructive inflammatory reactions [57]. In studies delivering small amounts of AAV vectors directly to the brain in Parkinson's disease [58-61], Canavan disease [62, 63] and late infantile neuronal ceroid lipofuscinosis [64], AAV vector administration was generally associated with minimal detectable immune responses to the capsid or the transgene in serum and peripheral blood mononuclear cells. The upper limit of vector dose that can be administered without breaking the immunologic unresponsiveness of the CNS is unclear, but we might hypothesise that our initial dose increased host cell permissiveness, without initiating a substantial immune response.

The mechanisms of AAV transduction have been reviewed previously, with N-linked galactose described as the primary receptor for AAV9 along with binding of a putative integrin and laminin receptors as co-receptors [65-67]. In brief, when AAV9 reaches a cell, it attaches to receptors/co-receptors and is endocytosed into the cell. Inside the endocytic vesicle, the virion travels towards the trans-Golgi network. During this trafficking phase, it goes through structural changes that expose a catalytic domain on the capsid. The virion then escapes into the cytosol and the capsid is imported through the nuclear pore complex into the nucleus in an importin B-dependent process. Here, the single stranded genome is ultimately released from the capsid. After release, it is converted to double stranded DNA and it persists as a circular episome, and linear or episomal concatemers. It is this final step of AAV9 transduction that permits expression of the transgene. Conversion into double stranded DNA (dsDNA) is often described as the rate-limiting step for AAV9 transduction, that restricts the efficiency, speed of onset and transgene expression. dsDNA conversion relies partially on host-cell DNA synthesis and vector concentration [68-71]. Augmentation of viral transduction can be achieved by improving the efficiency of double stranded DNA conversion, independently of vector titre. Current methods

for this include using DNA-damaging agents such as ultraviolet irradiation or hydroxyurea, or inhibition of specific host-cell factors. However, the clinical utility of such approaches is limited, due to the risk of mutagenic breaks and exacerbation of genotoxicity. Use of a self-complementary AAV however bypasses the need for second-strand synthesis by folding into a double stranded structure (via deletion of the D-sequence on one of the inverted terminal repeats). Further work is therefore required to elucidate if our dosing approach may have influenced the cellular machinery and/or expression kinetics or efficiency, or influenced proteasomal degradation pathways, to consequently enhance transduction. Indeed, we might reasonably hypothesise that a threshold exists whereby higher doses reach a level that is sufficient to transduce glial cells, however our finding of significant cortical astrocyte transduction following ICV administration may indicate other mechanisms at play. Our repeated dose regimen may have activated astrocytes and consequently made them more prone to take up gene vectors after consecutive injection. In future, including a bilateral group dosed within the same session would be pertinent to elucidate effects caused by dose versus schedule. Additional work may also seek to explore transduction levels of other cell types such as oligodendrocytes or interneurons and explore their contribution to viral genome load, and whether this might explain increases. Due to issues with GFP visualisation, it was not possible to assess intensity of GFP in motor neurons here, however, in future, this would be of interest, since we might hypothesise that more viral genomes are incorporated and this might help to explain the discrepancy seen between cell numbers and viral copy number. Increases in GFP expression could explain increases in copy number despite transduced cell numbers appearing similar.

Overall, further work is required to understand the complex mechanisms by which repeated AAV9 delivery across consecutive days can increase viral load in the spinal cord, and the utility, if any, of such an approach. The lack of cortical transduction remains surprising and warrants further investigation.

8. References

1. Asokan, A., D.V. Schaffer, and R.J. Samulski, *The AAV vector toolkit: poised at the clinical crossroads.* Mol Ther, 2012. **20**(4): p. 699-708.

2. Foust, K.D. and B.K. Kaspar, *Over the barrier and through the blood: to CNS delivery we go.* Cell Cycle, 2009. **8**(24): p. 4017-8.
3. Duque, S., et al., *Intravenous administration of self-complementary AAV9 enables transgene delivery to adult motor neurons.* Mol Ther, 2009. **17**(7): p. 1187-96.
4. Gray, S.J., et al., *Preclinical differences of intravascular AAV9 delivery to neurons and glia: a comparative study of adult mice and nonhuman primates.* Mol Ther, 2011. **19**(6): p. 1058-69.
5. Dismuke, D.J., L. Tenenbaum, and R.J. Samulski, *Biosafety of recombinant adeno-associated virus vectors.* Curr Gene Ther, 2013. **13**(6): p. 434-52.
6. Bevan, A.K., et al., *Systemic gene delivery in large species for targeting spinal cord, brain, and peripheral tissues for pediatric disorders.* Mol Ther, 2011. **19**(11): p. 1971-80.
7. Fu, H., et al., *Correction of neurological disease of mucopolysaccharidosis IIIB in adult mice by rAAV9 trans-blood-brain barrier gene delivery.* Mol Ther, 2011. **19**(6): p. 1025-33.
8. Kotulska, K., A. Fattal-Valevski, and J. Haberlova, *Recombinant Adeno-Associated Virus Serotype 9 Gene Therapy in Spinal Muscular Atrophy.* Front Neurol, 2021. **12**: p. 726468.
9. Peters, C.W., C.A. Maguire, and K.S. Hanlon, *Delivering AAV to the Central Nervous and Sensory Systems.* Trends Pharmacol Sci, 2021. **42**(6): p. 461-474.
10. Samaranch, L., et al., *Adeno-associated virus serotype 9 transduction in the central nervous system of nonhuman primates.* Hum Gene Ther, 2012. **23**(4): p. 382-9.
11. Mingozzi, F. and K.A. High, *Immune responses to AAV vectors: overcoming barriers to successful gene therapy.* Blood, 2013. **122**(1): p. 23-36.
12. Chandler, R.J., et al., *Vector design influences hepatic genotoxicity after adeno-associated virus gene therapy.* J Clin Invest, 2015. **125**(2): p. 870-80.
13. Stoica, L., et al., *Gene transfer to the CNS using recombinant adeno-associated virus.* Curr Protoc Microbiol, 2013. **Chapter 14**: p. 14D 5 1-14D 5 18.
14. Hollidge, B.S., et al., *Kinetics and durability of transgene expression after intrastriatal injection of AAV9 vectors.* Front Neurol, 2022. **13**: p. 1051559.
15. Iannitti, T., et al., *Translating SOD1 Gene Silencing toward the Clinic: A Highly Efficacious, Off-Target-free, and Biomarker-Supported Strategy for fALS.* Mol Ther Nucleic Acids, 2018. **12**: p. 75-88.
16. Saunders, N.R., et al., *Recent Developments in Understanding Barrier Mechanisms in the Developing Brain: Drugs and Drug Transporters in Pregnancy, Susceptibility or Protection in the Fetal Brain?* Annu Rev Pharmacol Toxicol, 2019. **59**: p. 487-505.
17. Saunders, N.R., S.A. Liddelow, and K.M. Dziegielewska, *Barrier mechanisms in the developing brain.* Front Pharmacol, 2012. **3**: p. 46.

18. Bucher, T., et al., *Intracisternal delivery of AAV9 results in oligodendrocyte and motor neuron transduction in the whole central nervous system of cats.* Gene Ther, 2014. **21**(5): p. 522-8.
19. Kilkenny, C., et al., *Improving bioscience research reporting: the ARRIVE guidelines for reporting animal research.* PLoS Biol, 2010. **8**(6): p. e1000412.
20. Glascock, J.J., et al., *Delivery of therapeutic agents through intracerebroventricular (ICV) and intravenous (IV) injection in mice.* J Vis Exp, 2011(56).
21. Lamprecht, M.R., D.M. Sabatini, and A.E. Carpenter, *CellProfiler: free, versatile software for automated biological image analysis.* Biotechniques, 2007. **42**(1): p. 71-5.
22. Stirling, D.R., et al., *CellProfiler 4: improvements in speed, utility and usability.* BMC Bioinformatics, 2021. **22**(1): p. 433.
23. Jan, A., et al., *Gene Transfer in Rodent Nervous Tissue Following Hindlimb Intramuscular Delivery of Recombinant Adeno-Associated Virus Serotypes AAV2/6, AAV2/8, and AAV2/9.* Neurosci Insights, 2019. **14**: p. 1179069519889022.
24. Foust, K.D., et al., *Intravascular AAV9 preferentially targets neonatal neurons and adult astrocytes.* Nat Biotechnol, 2009. **27**(1): p. 59-65.
25. Shinohara, Y., et al., *Effects of Neutralizing Antibody Production on AAV-PHP.B-Mediated Transduction of the Mouse Central Nervous System.* Mol Neurobiol, 2019. **56**(6): p. 4203-4214.
26. Schuster, D.J., et al., *Biodistribution of adeno-associated virus serotype 9 (AAV9) vector after intrathecal and intravenous delivery in mouse.* Front Neuroanat, 2014. **8**: p. 42.
27. Mattar, C.N., et al., *Systemic gene delivery following intravenous administration of AAV9 to fetal and neonatal mice and late-gestation nonhuman primates.* FASEB J, 2015. **29**(9): p. 3876-88.
28. Miyake, N., et al., *Global gene transfer into the CNS across the BBB after neonatal systemic delivery of single-stranded AAV vectors.* Brain Res, 2011. **1389**: p. 19-26.
29. Rahim, A.A., et al., *Intravenous administration of AAV2/9 to the fetal and neonatal mouse leads to differential targeting of CNS cell types and extensive transduction of the nervous system.* FASEB J, 2011. **25**(10): p. 3505-18.
30. Deverman, B.E., et al., *Cre-dependent selection yields AAV variants for widespread gene transfer to the adult brain.* Nat Biotechnol, 2016. **34**(2): p. 204-9.
31. Chan, K.Y., et al., *Engineered AAVs for efficient noninvasive gene delivery to the central and peripheral nervous systems.* Nat Neurosci, 2017. **20**(8): p. 1172-1179.
32. Nonnenmacher, M., et al., *Rapid evolution of blood-brain-barrier-penetrating AAV capsids by RNA-driven biopanning.* Mol Ther Methods Clin Dev, 2021. **20**: p. 366-378.
33. Bunuales, M., et al., *Characterization of brain transduction capability of a BBB-penetrant AAV vector in mice, rats and macaques reveals differences in expression profiles.* Gene Ther, 2024. **31**(9-10): p. 455-466.

34. Hudry, E., et al., *Liver injury in cynomolgus monkeys following intravenous and intrathecal scAAV9 gene therapy delivery.* Mol Ther, 2023. **31**(10): p. 2999-3014.
35. Agarwal, S., *High-dose AAV gene therapy deaths.* Nat Biotechnol, 2020. **38**(8): p. 910.
36. Chand, D., et al., *Hepatotoxicity following administration of onasemnogene abeparvovec (AVXS-101) for the treatment of spinal muscular atrophy.* J Hepatol, 2021. **74**(3): p. 560-566.
37. Hamilton, B.A. and J.F. Wright, *Challenges Posed by Immune Responses to AAV Vectors: Addressing Root Causes.* Front Immunol, 2021. **12**: p. 675897.
38. Hinderer, C., et al., *Severe Toxicity in Nonhuman Primates and Piglets Following High-Dose Intravenous Administration of an Adeno-Associated Virus Vector Expressing Human SMN.* Hum Gene Ther, 2018. **29**(3): p. 285-298.
39. Whiteley, L.O., *An Overview of Nonclinical and Clinical Liver Toxicity Associated With AAV Gene Therapy.* Toxicol Pathol, 2023. **51**(7-8): p. 400-404.
40. Abdel-Misih, S.R. and M. Bloomston, *Liver anatomy.* Surg Clin North Am, 2010. **90**(4): p. 643-53.
41. Racanelli, V. and B. Rehermann, *The liver as an immunological organ.* Hepatology, 2006. **43**(2 Suppl 1): p. S54-62.
42. Keeler, G.D., D.M. Markusic, and B.E. Hoffman, *Liver induced transgene tolerance with AAV vectors.* Cell Immunol, 2019. **342**: p. 103728.
43. Boutin, S., et al., *Prevalence of serum IgG and neutralizing factors against adeno-associated virus (AAV) types 1, 2, 5, 6, 8, and 9 in the healthy population: implications for gene therapy using AAV vectors.* Hum Gene Ther, 2010. **21**(6): p. 704-12.
44. Calcedo, R., et al., *Adeno-associated virus antibody profiles in newborns, children, and adolescents.* Clin Vaccine Immunol, 2011. **18**(9): p. 1586-8.
45. Meyer, K., et al., *Improving single injection CSF delivery of AAV9-mediated gene therapy for SMA: a dose-response study in mice and nonhuman primates.* Mol Ther, 2015. **23**(3): p. 477-87.
46. Bey, K., et al., *Intra-CSF AAV9 and AAVrh10 Administration in Nonhuman Primates: Promising Routes and Vectors for Which Neurological Diseases?* Mol Ther Methods Clin Dev, 2020. **17**: p. 771-784.
47. Bell, P., et al., *Motor neuron transduction after intracisternal delivery of AAV9 in a cynomolgus macaque.* Hum Gene Ther Methods, 2015. **26**(2): p. 43-4.
48. Kumagai, S., et al., *Early distribution of(18) F-labeled AAV9 vectors in the cerebrospinal fluid after intracerebroventricular or intracisternal magna infusion in non-human primates.* J Gene Med, 2023. **25**(1): p. e3457.
49. Belur, L.R., et al., *Comparative Effectiveness of Intracerebroventricular, Intrathecal, and Intranasal Routes of AAV9 Vector Administration for Genetic Therapy of Neurologic Disease in*

Murine Mucopolysaccharidosis Type I. Front Mol Neurosci, 2021. **14**: p. 618360.
50. Mueller, C., et al., *SOD1 Suppression with Adeno-Associated Virus and MicroRNA in Familial ALS.* N Engl J Med, 2020. **383**(2): p. 151-158.
51. Hinderer, C., et al., *Evaluation of Intrathecal Routes of Administration for Adeno-Associated Viral Vectors in Large Animals.* Hum Gene Ther, 2018. **29**(1): p. 15-24.
52. Hordeaux, J., et al., *Adeno-Associated Virus-Induced Dorsal Root Ganglion Pathology.* Hum Gene Ther, 2020. **31**(15-16): p. 808-818.
53. Garza, I.T., et al., *Expression and distribution of rAAV9 intrathecally administered in juvenile to adolescent mice.* Gene Ther, 2025. **32**(3): p. 189-196.
54. Ayers, J.I., et al., *Widespread and efficient transduction of spinal cord and brain following neonatal AAV injection and potential disease modifying effect in ALS mice.* Mol Ther, 2015. **23**(1): p. 53-62.
55. Matsuzaki, Y., et al., *Optimal different adeno-associated virus capsid/promoter combinations to target specific cell types in the common marmoset cerebral cortex.* Mol Ther Methods Clin Dev, 2024. **32**(4): p. 101337.
56. McLean, J.R., et al., *Widespread neuron-specific transgene expression in brain and spinal cord following synapsin promoter-driven AAV9 neonatal intracerebroventricular injection.* Neurosci Lett, 2014. **576**: p. 73-8.
57. Forrester, J.V., P.G. McMenamin, and S.J. Dando, *CNS infection and immune privilege.* Nat Rev Neurosci, 2018. **19**(11): p. 655-671.
58. Kaplitt, M.G., et al., *Safety and tolerability of gene therapy with an adeno-associated virus (AAV) borne GAD gene for Parkinson's disease: an open label, phase I trial.* Lancet, 2007. **369**(9579): p. 2097-105.
59. Marks, W.J., Jr., et al., *Safety and tolerability of intraputaminal delivery of CERE-120 (adeno-associated virus serotype 2-neurturin) to patients with idiopathic Parkinson's disease: an open-label, phase I trial.* Lancet Neurol, 2008. **7**(5): p. 400-8.
60. Marks, W.J., Jr., et al., *Gene delivery of AAV2-neurturin for Parkinson's disease: a double-blind, randomised, controlled trial.* Lancet Neurol, 2010. **9**(12): p. 1164-1172.
61. Christine, C.W., et al., *Safety and tolerability of putaminal AADC gene therapy for Parkinson disease.* Neurology, 2009. **73**(20): p. 1662-9.
62. McPhee, S.W., et al., *Immune responses to AAV in a phase I study for Canavan disease.* J Gene Med, 2006. **8**(5): p. 577-88.
63. Leone, P., et al., *Long-term follow-up after gene therapy for canavan disease.* Sci Transl Med, 2012. **4**(165): p. 165ra163.
64. Worgall, S., et al., *Treatment of late infantile neuronal ceroid lipofuscinosis by CNS administration of a serotype 2 adeno-associated virus expressing CLN2 cDNA.* Hum Gene Ther, 2008. **19**(5): p. 463-74.

65. Shen, S., et al., *Terminal N-linked galactose is the primary receptor for adeno-associated virus 9.* J Biol Chem, 2011. **286**(15): p. 13532-40.
66. Bell, C.L., et al., *Identification of the galactose binding domain of the adeno-associated virus serotype 9 capsid.* J Virol, 2012. **86**(13): p. 7326-33.
67. Dhungel, B.P., C.G. Bailey, and J.E.J. Rasko, *Journey to the Center of the Cell: Tracing the Path of AAV Transduction.* Trends Mol Med, 2021. **27**(2): p. 172-184.
68. Hauck, B., et al., *Intracellular viral processing, not single-stranded DNA accumulation, is crucial for recombinant adeno-associated virus transduction.* J Virol, 2004. **78**(24): p. 13678-86.
69. Fisher, K.J., et al., *Transduction with recombinant adeno-associated virus for gene therapy is limited by leading-strand synthesis.* J Virol, 1996. **70**(1): p. 520-32.
70. Ferrari, F.K., et al., *Second-strand synthesis is a rate-limiting step for efficient transduction by recombinant adeno-associated virus vectors.* J Virol, 1996. **70**(5): p. 3227-34.
71. Maurer, A.C. and M.D. Weitzman, *Adeno-Associated Virus Genome Interactions Important for Vector Production and Transduction.* Hum Gene Ther, 2020. **31**(9-10): p. 499-511.

9. Author Contributions

A.J. Mole: Data curation, formal analysis, investigation, methodology, project administration, software, supervision, visualisation, writing – original draft, writing – review & editing
C.F. Sander: Data curation, formal analysis, methodology, software, visualisation, writing – review & editing
A.R. Parmar: Methodology, validation, visualisation, writing – review & editing
A.J. Wlliams: Methodology, visualisation, writing – review & editing
M. Azzouz: Conceptualization, funding acquisition, supervision, writing – review & editing
G.M. Hautbergue: Conceptualization, funding acquisition, supervision, writing – review & editing
P.J. Shaw: Conceptualization, funding acquisition, supervision, writing – review & editing
L. Ferraiuolo: Conceptualization, funding acquisition, supervision, writing – review & editing
R.J. Mead: Conceptualization, funding acquisition, project administration, resources, supervision, writing – review & editing

10. Data Availability

The datasets generated during and analysed during the current study are available from the corresponding author on reasonable request.

11. Funding Declaration

This work was supported by the MND Association and MND Scotland [2023/MNDS/6501/791MEA].

12. Conflicts of Interest

None to declare.